Generation of optical domain-wall structures from modulational instability in a bimodal fiber

S. Pitois, G. Millot, and P. Grelu
Laboratoire de Physique, Université de Bourgogne, 9 Avenue Savary, Boîte Postale 47 870, F-21078 Dijon, France

M. Haelterman
Service d'Optique et Acoustique, Université Libre de Bruxelles, 50 Avenue Roosevelt, Code Postal 194/5, B-1050 Bruxelles, Belgium
(Received 21 December 1998)

We study experimentally modulational instability in a normally dispersive bimodal fiber under modal group-velocity-matching conditions. In the strong pump depletion regime, higher order sideband harmonics detected in the output spectra as well as autocorrelation measurements reveal the formation of subpicosecond domain-wall structures. Across these temporal structures the electromagnetic field distribution switches abruptly between the two transverse modes of the fiber. These structures are reminiscent of the so-called domain-wall soliton. Our results constitute therefore an experimental indication of the existence of this fundamental soliton. [S1063-651X(99)02507-6]

PACS number(s): 42.81.Dp, 42.65.Ky, 42.65.Re

I. INTRODUCTION

Modulational instability (MI) in optical fibers is a quasidegenerate parametric four-wave-mixing process for which the phase-matching condition results naturally from a compensation of dispersion by the Kerr nonlinearity of silica [1]. In the scalar approximation of the electromagnetic field, light propagation in optical fibers is ruled by the nonlinear Schrödinger (NLS) equation. It is well known in this case that the positive Kerr nonlinearity of silica can only compensate for negative (anomalous) dispersion in order to achieve phase matching of the MI process [1]. When accounting for the vector nature of light, an extra degree of freedom is added to the phase-matching condition and the positive Kerr nonlinearity can compensate for both negative and positive dispersions. This extension of the domain of modulational instability to the positive (normal) dispersion regime has been first described by Berkhoer and Zakharov in 1970 for the case of isotropic Kerr media [2]. The description has been generalized to birefringent Kerr media by Wabnitz who called polarization modulational instability (PMI) the vector MI process that occurs in the normal dispersion regime [3]. A few years later, Haelterman and Sheppard showed that a fundamental vector soliton is associated with MPI in the same way as the well-known NLS sech-shaped soliton is associated with scalar MI [4]. This fundamental vector soliton is a localized structure of the dark type across which the electromagnetic field switches between the two orthogonal nonlinear polarization eigenstates of the Kerr medium [5]. For this reason it has been called a polarization domain-wall soliton. This fundamental soliton has never, to the best of our knowledge, been observed experimentally up to now because of the difficulty to generate it and propagate it in fibers. The main obstacle is that its propagation requires that the polarization state does not change along the fiber axis or, in other words, that the birefringence is zero or maintained weak and constant over long distances. Because this difficulty is inherent to the vector nature of this soliton, we decided to investigate another physical system that is liable to sustain domain-wall solitons.

The system under consideration here is a bimodal fiber in which the group velocities of the two modes are equal in order to fulfill the conditions of existence of the domain walls. Indeed, light propagation in such a fiber is ruled by two NLS equations that are coupled through cross-phase modulation between the two modes. According to the theory of Berkhoer and Zakharov, since cross-phase modulation between orthogonal modes is in general stronger than self-phase modulation, we can expect that MI occurs in the normal dispersion regime and that, *a fortiori*, the associated domain-wall soliton exists. We have discussed this problem in detail in a recent paper where we reported, through spectral measurements, the occurrence of MI under modal group-velocity-matching conditions in a normally dispersive bimodal fiber [6]. Let us note that coupling between two light sources of different wavelength also leads to cross-phase modulation (CPM) larger than self-phase modulation [7], but a special *W*-type single-mode fiber must be used to fulfill the condition of identical group velocities between the two modes [8].

Our scope here is to extend our first experimental work in a bimodal fiber to the study of the temporal patterns generated by MI along the fiber in the strong pump depletion regime. We show that the generated patterns are periodic trains of domain-wall structures. The domain walls in this case separate domains in which the electromagnetic fields differ in their transverse distributions since these are nothing but the two orthogonal transverse modes of the fiber. In other words, quite remarkably, MI is responsible for a periodic alternation of the transverse field configuration between the two transverse modal distributions of the fiber at the picosecond time scale. It must be noted that these domain-wall structures are not the so-called domain-wall solitons since they are not stationary. Indeed, as in the scalar case, MI leads to recurrent dynamics [9,10] and the patterns that are generated continuously evolve along the propagation axis. As a result, the domain-wall structures are observed only at a pre-

cise propagation distance that depends on the initial pump power. However, as shown in a detailed discussion in Ref. [4], the periodic structures formed through a MI process are intimately related to the soliton associated with this process. We can therefore, reasonably consider that the domain-wall structures observed here constitute an indirect but valuable proof of the existence of the domain-wall soliton.

II. THEORY

We consider a circular bimodal silica fiber in the normal dispersion regime under single-frequency pumping, where two pump waves propagate along the first linearized LP_{01} and LP_{11} modes of the fiber, respectively. Wave propagation in such a fiber is ruled by two incoherently coupled nonlinear Schrödinger equations [1]

$$\frac{\partial E_j}{\partial z}+(-1)^j\frac{\delta}{2}\frac{\partial E_j}{\partial t}+\frac{1}{2}i\beta_j''\frac{\partial^2 E_j}{\partial t^2} =i\gamma_j(|E_j|^2+2r_j|E_{1-j}|^2)E_j, \quad j=0,1, \qquad (1)$$

where E_j are the slowly varying field envelopes of the two modes, β_j'' are the group-velocity dispersion coefficients of each mode, and $\delta=1/V_{g0}-1/V_{g1}$ is the group-velocity mismatch between the two modes with V_{gj} the group velocity of the LP_{j1} mode. The nonlinear coefficients γ_j are defined by $\gamma_j=2\pi n_2/(\lambda A_j)$ where λ is the pump wavelength, $n_2=3.2\times10^{-16}\,\mathrm{cm^2/W}$ is the nonlinear refractive index, and A_j are the effective core areas of the modes, $A_j=(\int|F_j|^2dS)^2/\int|F_j|^4dS$ where F_j are the transverse field distributions of the LP_{j1} modes. The nonuniform transverse field distributions are responsible for the weighting factors r_j of the cross-phase modulation coefficients in Eq. (1),

$$r_j=A_j\int|F_0|^2|F_1|^2dS\Big/\left(\int|F_0|^2dS\int|F_1|^2dS\right).$$

All above coefficients relating to the characteristics of the fiber were calculated for an ideal circular step-index fiber by using standard procedures of linear waveguide theory (including Sellmeier relations for the contribution of material dispersion). The fiber parameters at critical wavelength $\lambda=\lambda_c\simeq626.5\,\mathrm{nm}$ where the two modes have the same group velocity (i.e., $\delta=0$) were the following: core index $n_{co}=1.457$, cladding index $n_{cl}=1.4484$, CPM coefficients $r_0=0.55$ and $r_1=0.705$, group-velocity-dispersion (GVD) parameters $\beta_0''=52.9\,\mathrm{ps^2\,km^{-1}}$ and $\beta_1''=63.4\,\mathrm{ps^2\,km^{-1}}$, nonlinear coefficients $\gamma_0=30.3\,\mathrm{W^{-1}\,km^{-1}}$ and $\gamma_1=23.6\,\mathrm{W^{-1}\,km^{-1}}$ [6]. The core radius of the fiber was taken to be $a=1.8892\,\mu\mathrm{m}$ so as to fit at best the theoretical predictions with the experimental results. As regards this point, it is worth noting that the core radius a and the cladding index are the only fit parameters in the model.

Equation (1) has been used to model our recent experiment on MI in the bimodal fiber [6]. An excellent agreement has been obtained between theory and the measured MI spectra. For the sake of clarity of the presentation, we briefly recall here the main results of the theoretical developments. MI is examined by a standard linear stability analysis of the continuous-wave (cw) solutions of the coupled NLS equations (1). One of the important results of this analysis is that

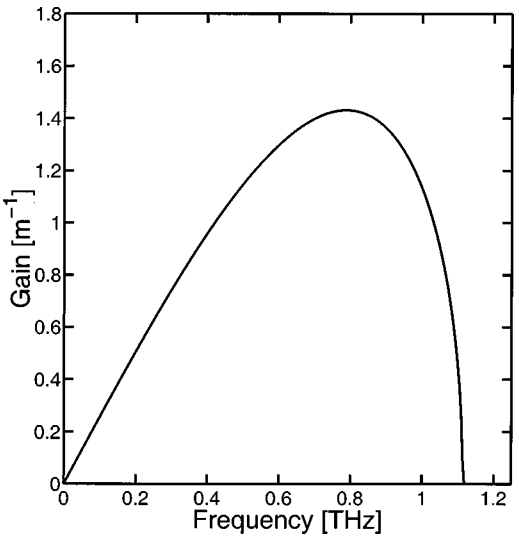

FIG. 1. Theoretical MI gain ($\mathrm{m^{-1}}$) spectrum of the bimodal fiber at zero group-velocity mismatch ($\lambda=\lambda_c$). The pump power in both modes is $P_0=P_1=110\,\mathrm{W}$.

it shows the onset of MI in the normal dispersion regime at the wavelength where the group-velocity difference between the LP_{01} and the LP_{11} modes vanishes, i.e., $\delta=0$ [6]. This result reveals that the bimodal fiber allows us to reproduce the physical conditions that constitute the basis of Berkhoer and Zakharov's theory of PMI in isotropic Kerr media. As shown in that theory, MI with velocity-matched waves in the normal dispersion regime is possible only if cross-phase modulation between the waves is stronger than self-phase modulation (see also Ref. [12] for a detailed analysis). In Eq. (1) this condition is expressed through the inequality $4r_0r_1>1$, which is fulfilled with the bimodal fiber of our experiment [6]. When $\delta=0$ and $4r_0r_1>1$, the MI gain spectra have the shape of a single paraboliclike lobe that extends from $\Omega=0$ to a certain frequency $\Omega=\Omega_{max}$ that depends on the pump power in each mode, P_0 and P_1 (see Fig. 1). The maximum gain is obtained at the frequency $\Omega_{opt}\simeq\Omega_{max}/\sqrt{2}$. For instance, with the fiber parameters defined above, we find $\Omega_{max}=1.12\,\mathrm{THz}$ for $P_0=P_1=110\,\mathrm{W}$. Another important conclusion of the linear stability analysis is drawn from the study of the eigenvectors associated with the unstable eigenvalues [4]. The peculiar symmetry of the eigenvectors indicates that MI induces two π-out-of-phase periodic patterns in both mode envelopes as was first described in Ref. [11]. Consequently, the mode envelopes form an interlaced structure that in the strong pump depletion regime can naturally be expected to lead, as in the case of PMI [4], to the formation of domain-wall structures.

We verified this scenario by integrating Eq. (1) with identical modal group velocities ($\delta=0$) by means of a standard numerical code based on the split-step Fourier method. In the experiment we seeded MI through the injection of a weak anti-Stokes signal along with the pump waves. Since, by definition of MI the parametric wave-mixing process involving the Stokes wave is automatically phase matched, the Stokes wave grows and reaches very rapidly the amplitude of the anti-Stokes wave. Therefore, the system evolution will follow very closely the predictions of the standard linear stability analysis (based on symmetric Stokes and anti-Stokes

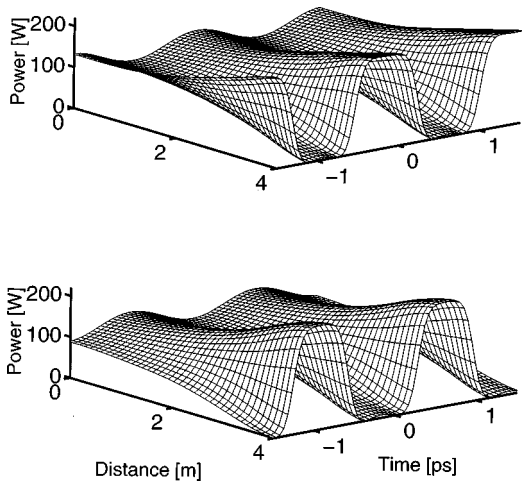

FIG. 2. Evolution over 4 m of the intensity profiles of the two modes at zero group-velocity mismatch. The initial pump powers are $P_0 = P_1 = 110\,\mathrm{W}$ and the seed parameter is $\rho = 0.1$.

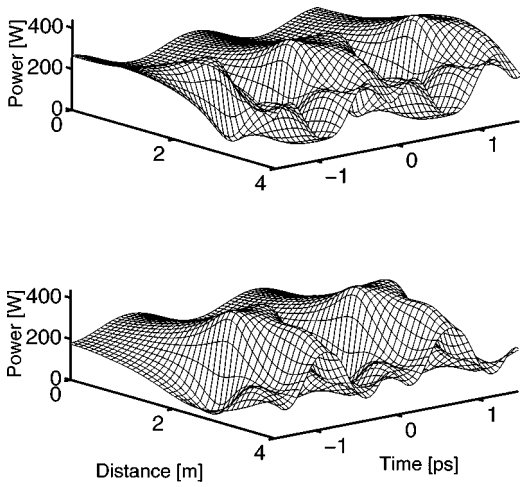

FIG. 3. Evolution over 4 m of the intensity profiles of the two modes at zero group-velocity mismatch. The initial pump powers are $P_0 = P_1 = 220\,\mathrm{W}$ and the seed parameter is $\rho = 0.1$.

excitation) presented above. The advantage of seeding the instability is that we can choose the modulation frequency. If this frequency is sufficiently small compared to the optimal MI frequency Ω_{opt}, many sidebands fall within the MI gain bandwidth and can therefore grow to form highly structured periodic envelopes. In this way we can expect the formation of periodic trains of well isolated domain-wall structures. To verify this prediction numerically, we then used the following initial conditions to integrate Eq. (1):

$$E_j(z=0,t) = \sqrt{P_j}\,[1 + (-1)^j \rho \exp(i\Omega t)], \qquad (2)$$

where the seeding parameter ρ is the initial signal-to-pump field amplitude ratio and Ω is the frequency difference between the anti-Stokes and pump waves or, in other words, the modulation frequency. Figure 2 shows a typical example of evolution of the temporal power profiles of the two fiber modes. The input cw pump powers are taken identical in each mode, $P_0 = P_1 = 110\,\mathrm{W}$, the modulation frequency is $\Omega = 0.648\,\mathrm{THz}$, while the seeding parameter is $\rho = 0.1$. Note that the modulation frequency is in this case smaller than the optimal MI frequency $\Omega_{\mathrm{opt}} = 0.79\,\mathrm{THz}$. This condition is required to get the growth of a sufficiently large number of sidebands so that the envelope modulation reaches a depth that is of about 100% and the resulting π-out-of-phase periodic patterns take the shape of nearly square-shaped pulse trains. In other words, sharp domain-wall temporal structures are generated and, accordingly, the electromagnetic field distribution in the fiber switches periodically between the two transverse modes of the fiber. Periodic switching occurs at a rate of 0.648 THz with a rise time of 200 fs corresponding to an increase from 10% to 90% of the intensity of one of the modes. We define the width of the domain-wall structures as being this rise time. Let us notice that the precise value of the seed amplitude ($\rho = 0.1$) has been chosen so that the domain-wall structures are formed in the simulation exactly at the propagation distance of 4 m corresponding to the fiber length considered in the experiment. Note finally that, although sharp square structures with almost 100% contrast are generated by MI, the total intensity profile of the field pattern remains almost constant since the envelopes of both modes are complementary and form an interlaced structure.

As mentioned in the introduction, the domain-wall structures in Fig. 2 are not the solitons associated with the MI process. Indeed, since the coupled NLS equations are conservative, the dynamics of MI is recurrent as in the scalar NLS equation [9,10]. As a result, after the formation of deeply modulated periodic patterns, energy of the sidebands goes back to the pump and the field envelopes flatten and take progressively their initial shape before being modulated again. This dynamical feature has been described in Ref. [4] in the case of PMI in isotropic Kerr media. It shows that the periodic patterns generated through MI are not stationary and can therefore by no means be considered as periodic trains of solitons. This important point is illustrated in Fig. 3, which shows the evolution of the field power temporal profiles for a larger pump power than in Fig. 2. We see that after the formation of domain-wall structures (at $z \simeq 2.5\,\mathrm{m}$) analogous to those of Fig. 2, the field follows a complex erratic evolution in which higher modulation frequencies appear. This behavior differs significantly from the recurrent dynamics described in Ref. [4] simply because we consider here an initial modulation frequency smaller than the optimal MI frequency. In this case a large number of sidebands appear in the system contrary to the situation analyzed in Ref. [4] where only one Stokes anti-Stokes sideband pair was considered. It is the presence of more than one sideband pair in the MI spectrum that leads to complex and apparently chaotic dynamical behaviors.

Despite the fact that the generated patterns are not stationary periodic soliton trains, their structure is obviously reminiscent of the domain-wall soliton. To support this idea we first have to show that Eq. (1) possesses domain-wall soliton solutions when the group velocities of the two modes are identical ($\delta = 0$). Let us consider steady state solutions of Eq. (1) in the form $E_j = e_j(t)\exp(i\beta_j z)$ [4,8,13]. Substitution of this expression into Eq. (1) with $\delta = 0$ leads to a set of coupled ordinary differential equations:

$$\frac{1}{2}\,\beta_j'' \frac{d^2 e_j}{dt^2} = -\beta_j e_j + \gamma_j e_j^3 + 2 r_j \gamma_j e_j e_{1-j}^2, \quad j = 0,1. \qquad (3)$$

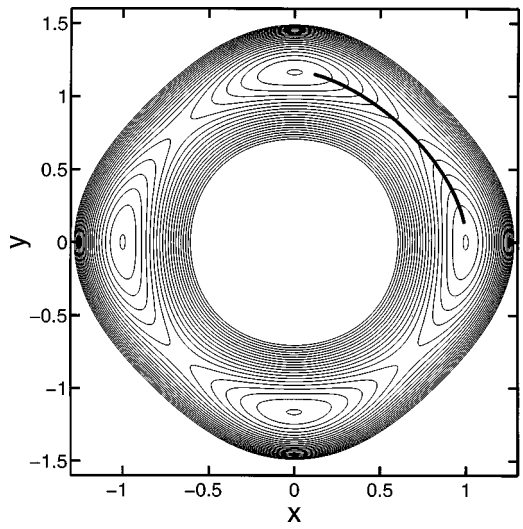

FIG. 4. Contour lines of the potential $V(x,y)$. The thick line shows the oscillatory motion corresponding to the periodic train of domain-wall solitons.

The change of variables $x=e_0(\gamma_0/\beta_0)^{1/2}$, $y=e_1[r_0\gamma_0^2\beta_1''/(r_1\gamma_1\beta_0\beta_0'')]^{1/2}$, and $\tau=t(\beta_0/\beta_0'')^{1/2}$, transforms Eqs. (3) into

$$\ddot{x}=-2x+2x^3+4r\kappa xy^2,$$

$$\ddot{y}=-2\beta y+2\kappa^2y^3+4r\kappa x^2y, \tag{4}$$

where $\beta=\beta_1\beta_0''/(\beta_0\beta_1'')$ is a free wave parameter and $\kappa=\sqrt{r_1}\gamma_1\beta_0''/(\sqrt{r_0}\gamma_0\beta_1'')$, $r=\sqrt{r_0r_1}$ are material-dependent parameters. The dots denote derivatives with respect to time τ. Equations (4) are similar to the equation of motion in the plane (x,y) of a unit mass in the two-dimensional potential $V=x^2+\beta y^2-x^4/2-\kappa^2y^4/2-2r\kappa x^2y^2$. As shown in Fig. 4, this potential possesses four maxima corresponding to the fixed points of Eqs. (4) i.e., $x=\pm1$, $y=0$, where $V=V_1=1/2$ and $x=0$, $y=\pm\sqrt{\beta}/\kappa$, where $V=V_2=\beta^2/2\kappa^2$. Domain-wall solitons correspond to separatrix trajectories connecting pairs of adjacent maxima [5]. They therefore only exist if the four potential maxima take the same value $V_1=V_2$, that is, when $\beta_1/\beta_0=(\gamma_1/\gamma_0)^{1/2}$. Periodic trains of domain-wall solitons correspond to oscillatory motions of the unit mass between two adjacent maxima (see Fig. 4) [4]. Such solutions can be easily found by means of a standard numerical shooting technique. An example of a periodic train of domain-wall solitons is shown in Figs. 5(a) and 5(b) together with the patterns generated by MI with the parameters $P_0=P_1=110\,\mathrm{W}$, $\Omega=0.648\,\mathrm{THz}$, $\rho=0.1$, and a propagation length of $L=4\,\mathrm{m}$. The intensity profiles of both coupled wave pairs are very similar. In particular, the widths of both domain-wall structures are almost identical. In fact the two waves only differ significantly in their phase profiles. While the phase profile of the domain-wall solitons is rigorously flat, the phase profile of the MI-induced pattern exhibits large variations [see Figs. 5(c) and 5(d)], which explains why these patterns are nonstationary. However, on the basis of the above analysis, we can reasonably state that the experimental observation of the π-out-of-phase MI-induced periodic patterns constitute a valuable proof of the existence of the temporal domain-wall soliton. The scope of the experiment described in the next section is to establish this proof.

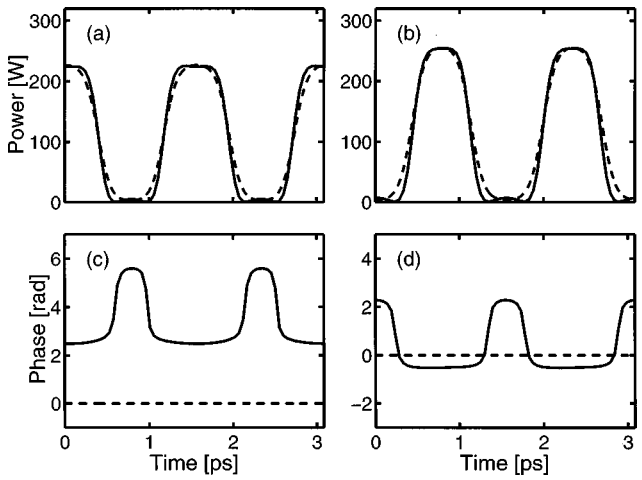

FIG. 5. (a), (b) Intensity profiles of both modes after propagation over 4 m with the parameters of Fig. 2. The dashed lines show the intensity profiles of the exact domain-wall soliton trains calculated by the shooting method. (c), (d) Phase profiles of the periodic signals shown in (a) and (b).

III. EXPERIMENT

We performed our experiment on MI with a standard telecommunication fiber whose cutoff wavelength for mode LP_{11} is 790 nm. The experimental setup is depicted sche-

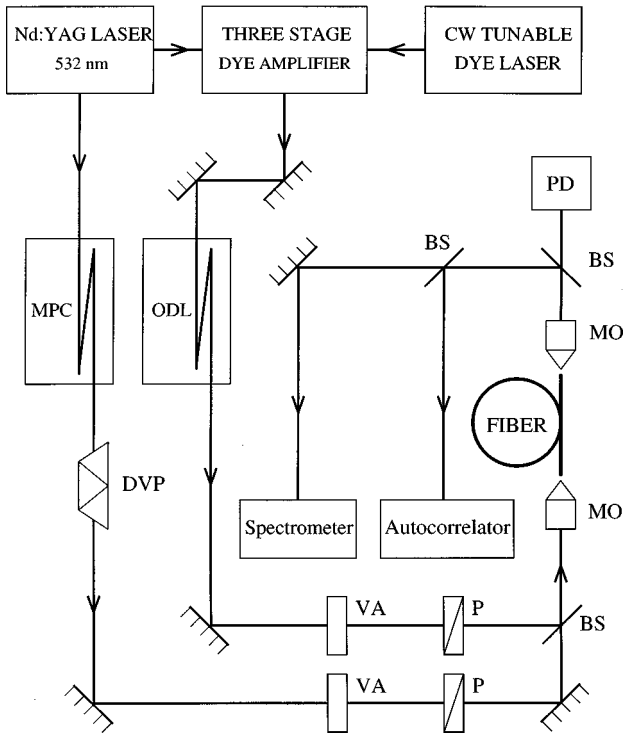

FIG. 6. Schematic of the experimental setup used for the study of induced MI in the bimodal fiber. MPC, multiple-pass cell; ODL, optical delay line; DVP, direct vision prism; VA, variable attenuator; P, glan polarizer; BS beam splitter; MO, 20× microscope objective; PD, photodiode.

matically in Fig. 6. Quasi-cw conditions were ensured by using nanosecond pulses delivered for the pump and the anti-Stokes signal by two distinct laser sources. In this way more than three orders of magnitude separate the pulse duration from the characteristic modulation period of MI. The pump beam was obtained from a single-mode tunable dye laser amplified by a frequency-doubled injection-seeded Nd:YAG laser at 532 nm operating at the repetition rate of 25 Hz. The signal pulse was obtained by frequency shifting an intense beam from the Nd:YAG laser. The frequency shift resulted from the self-stimulated Raman effect taking place in carbon dioxide confined in a multiple-pass chamber at a pressure of 1.7×10^5 Pa. The resulting second Stokes wave (shifted by 2776 cm^{-1} from the input laser frequency) was filtered out with a direct vision prism and used as the signal wave. Synchronization between the signal and pump pulses was achieved by means of an optical delay line placed in the pump beam. Pump and signal beams with parallel polarizations and adjustable powers were obtained by means of two variable attenuators followed by two Glan polarizers. Both beams were combined through a beam splitter and focused with a 20× microscope objective in 4 m of bimodal fiber. After propagation through the fiber, light was first collimated and then split into three different beams. Peak powers were measured with a calibrated photodiode with an accuracy of about 15% whereas light was spectrally and temporally analyzed with a monochromator and a home-built background-free second-harmonic generation autocorrelator. Note that, due to the low powers obtained at the output of the system, an acceptable signal-to-noise ratio in the autocorrelation measurements requires several thousands of shots to scan about 10 ps of the pulse profile. On the other hand, the autocorrelator resolution is of about 70 fs and hence allowed us to observe comfortably the MI-induced structures. The temporal widths of the pump and signal pulses were determined by measuring the second-harmonic generation efficiency of each beam by comparison with the corresponding efficiency obtained with a reference pulse of identical energy and known duration. For such a calibration, collimation of each beam through a short piece of optical fiber ensured minimum waist size variations in the doubling crystal. The signal wavelength, fixed by the Raman shift, was $\lambda_s=624.54$ nm, whereas the pump wavelength was adjusted to $\lambda=625.33\,\text{nm}\simeq\lambda_c$ corresponding to group-velocity matching in the bimodal fiber. These wavelengths correspond to a modulation frequency of $\Omega=0.648$ THz. The critical wavelength has been determined with an accuracy of about 1 nm from measurements of the optimal modulation frequency resulting from spontaneous MI for a wide range of pump wavelengths [6]. On the other hand, numerical simulations of Eqs. (1) with the initial conditions given by Eq. (2) show that the domain-wall structures are not significantly altered for pump wavelength detunings from the critical wavelength smaller than 2 nm. According to the usual linear stability analysis, the maximum spontaneous instability gain is obtained when the pump power is equally distributed among both modes ($P_0=P_1$). Thus we optimized the launching conditions in order to achieve nearly equal pump power in the two modes by maximizing the intensity of the noise-induced sidebands which appear for strong total pump power without seeding. The total pump power is then reduced without changing the launching conditions. On the other hand a perfect alignment of the signal with respect to the pump provides the launching conditions to be simultaneously optimized for the signal. Autocorrelation measurements of the LP_{01} mode alone was achieved after separating both modes by means of a LP_{11} mode stripper placed at the output end of the fiber.

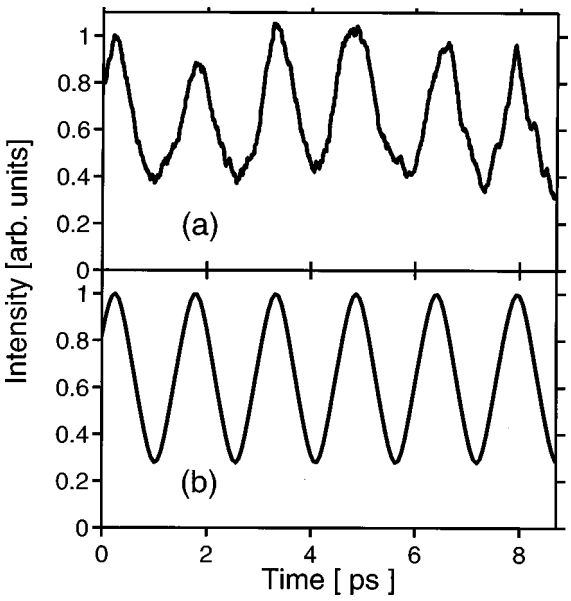

FIG. 7. (a) Experimental and (b) theoretical autocorrelation traces of the fundamental fiber mode (LP_{01}) at the fiber output with the parameters specified in the text.

According to the conclusions of the theoretical analysis presented in Sec. II, domain-wall structures appear at the output of the 4-m-long fiber only for particular values of $P_{\text{tot}}=P_0+P_1$ and ρ. Since we are dealing with pulsed waves, a perfect agreement between theory and experiment cannot be expected. Several measurements were performed for different values of P_{tot} and ρ chosen around the values predicted by the cw theory. The largest modulation depth of the autocorrelation trace was obtained for $P_0\simeq P_1=110$ W and $\rho=0.2$. Figure 7(a) shows the measured autocorrelation trace of the LP_{01} mode obtained with these parameters. As can be seen, the autocorrelation trace exhibits a modulation depth as large as 60% and a modulation period of about 1.54 ps in accordance with the initial modulation frequency $\Omega=0.648$ THz. Figure 7(b) shows the theoretical autocorrelation trace constructed with the intensity profiles obtained by numerical integration of Eq. (1) with the parameters of Fig. 5 by taking into account the pulsed nature of the pump and signal waves. The autocorrelation trace exhibits triangular peaks which confirm the presence of periodic square-shaped intensity profiles resulting from the MI-induced domain-wall structure formation. The slight discrepancy between the experimental and theoretical autocorrelation traces is explained by the power fluctuations and time jitter between pump and signal pulses which unavoidably reduced the contrast of the experimental trace. On the other hand fluctuations of the relative phase of the seed in the two modes may lead to a slight distortion of the domain-wall structure and hence to a reduction of the contrast of the autocorrelation trace. Note that if we do not use the mode stripper at the end of the fiber,

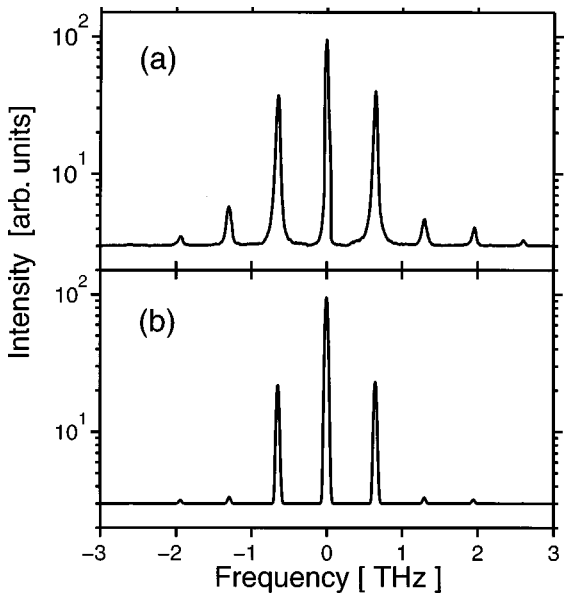

FIG. 8. (a) Experimental and (b) theoretical power spectra obtained at the fiber output in logarithmic scale (the spectra of both modes are superimposed).

the autocorrelation measurements exhibit flat intensity profiles. This result is important since it demonstrates that the two periodic patterns generated by MI in the orthogonal modes are complementary and form an interlaced structure, as predicted theoretically. The study of the output spectra also confirms the formation of domain-wall structures. Indeed, we verified a good agreement between the experimental spectra and the spectra observed by numerical simulations of the MI-induced domain-wall generation process. Figure 8 shows the calculated power spectra of the total field at the output end of the fiber (i.e., the spectra of both modes are here superimposed) for the same parameters as those of Fig. 7. In order to be able to compare theory and experiment, the apparatus function of the spectrometer, which is fairly well approximated by a Gaussian (with 0.04 nm full width at half maximum), was convoluted with the numerical spectrum. Note that the presence of higher order harmonics is a manifestation of the sharpness of the generated periodic square-wave structures. Let us mention that the experimental measurements of time evolution of the output intensities and phases in the two modes would require a second harmonic generation–frequency resolved optical gating (SHG-FROG) system [14] with very high sensitivity and the development of a phase-retrieval algorithm adapted for a high repetition rate pulse train. Such experimental and theoretical investigations are under way. From the above temporal and spectral measurements, we can reasonably infer that the MI process in the normally dispersive bimodal fiber leads to the formation of periodic domain-wall structures.

IV. CONCLUSION

In summary, by means of a bimodal fiber we have investigated modulational instability due to cross-phase modulation between two waves propagating with identical group velocities in the normal dispersion regime. From a fundamental point of view this problem is of interest since it allowed us to reproduce the key ingredients that are at the origin of polarization modulational instability in isotropic Kerr media. This fundamental instability of nonlinear light propagation had been predicted by Berkhoer and Zakharov in 1970 [2]. Its peculiarity is that the underlying four-wave-mixing process is phase matched through compensation of dispersion by the nonlinearity alone (contrary to what happens in previous experiments made on light propagation in birefringent fibers). Our theoretical and experimental study of the strong pump depletion regime demonstrates that modulational instability in the bimodal fiber leads to the formation of domain-wall structures. Temporal and spectral measurements indicate that these domain-wall structures are characterized by sharp and highly contrasted transitions between the transverse modes of the fibers. This type of pattern is reminiscent of the so-called domain-wall soliton that constitutes the fundamental vector soliton associated with CPM-induced MI in the normal dispersion regime [4]. Consequently, besides its uniqueness, the main interest of the observed phenomenon is that it constitutes a reliable indirect proof of the existence of this fundamental vector soliton that, to the best of our knowledge, up to now, has not yet been observed experimentally. However, due to the use of a bimodal fiber, the present work is far from any practical applications of the domain-wall solitons such as optical data transmissions [8,15]. To improve this situation, the same type of experiment should be achieved on CPM-induced MI involving waves of different frequencies [8] or polarizations [15]. This will be the scope of our future experimental research on this subject.

ACKNOWLEDGMENTS

The authors acknowledge E. Seve and S. Wabnitz for fruitful discussions. This research was supported by the Conseil Régional de Bourgogne, the Centre National de la Recherche Scientifique, the Ministère de la Recherche (France), and by the Fonds National de la Recherche Scientifique (Belgium) and the Inter-University Attraction Pole Program of the Belgian government under Grant No. P4-07.

[1] G. P. Agrawal, *Nonlinear Fiber Optics*, 2nd ed. (Academic, New York, 1995), Chap. 7, and references therein.
[2] A. L. Berkhoer and V. E. Zakharov, Zh. Eksp. Teor. Fiz. **58**, 903 (1970) [Sov. Phys. JETP **31**, 486 (1970)].
[3] S. Wabnitz, Phys. Rev. A **38**, 2018 (1988).
[4] M. Haelterman and A. Sheppard, Phys. Rev. E **49**, 3389 (1994).
[5] M. Haelterman and A. P. Sheppard, Opt. Lett. **19**, 96 (1994).
[6] G. Millot, S. Pitois, P. Tchofo Dinda, and M. Haelterman, Opt. Lett. **22**, 1686 (1997).
[7] G. P. Agrawal, Phys. Rev. Lett. **59**, 880 (1987).
[8] M. Haelterman and M. Badolo, Opt. Lett. **20**, 2285 (1995).
[9] E. Infeld, Phys. Rev. Lett. **47**, 717 (1981).
[10] N. N. Akhmediev, V. M. Eleonskii, and N. E. Kulagin, Theor. Math. Phys. **72**, 183 (1987).
[11] N. N. Akhmediev, V. I. Korneev, and N. V. Mitskevich, Izv.

Vyssh. Uchebn. Zaved. Radiofiz. **34**, 84 (1991).
[12] P. Tchofo Dinda, G. Millot, E. Seve, and M. Haelterman, Opt. Lett. **21**, 1640 (1996).
[13] M. Haelterman and A. Sheppard, Phys. Lett. A **185**, 265 (1994).
[14] K. W. Delong, R. Trebino, J. Hunter, and W. E. White, J. Opt. Soc. Am. B **11**, 2206 (1994).
[15] M. Haelterman, Electron. Lett. **30**, 1510 (1994).